Transport and Retention in an Upwelling Region: The role of across-shelf structure.

Moninya Roughan [a,*],

[a] *Scripps Institution of Oceanography, University of California San Diego, USA.*

Newell Garfield [b],

[b] *Romberg Tiburon Center, San Francisco State University, USA.*

John Largier [c],

[c] *Bodega Marine Laboratory, University of California Davis, USA.*

Edward Dever [d],

[d] *COAS, Oregon State University, USA.*

Clive Dorman [a], Dwight Peterson [b] and Jeff Dorman [b]

Preprint submitted to Deep Sea Research *15 June 2006*

Abstract

The paradox of upwelling is the relationship between strong wind forcing, nutrient enrichment and shelf productivity. Here we investigate how across-shelf structure in velocity and hydrography plays a role in the retention (inshore) and export (offshore) of particles such as nutrients, plankton and larvae.

We examine the spatial structure of the coastal currents during wind-driven upwelling and relaxation on the northern Californian Shelf. The field work was conducted as part of the Wind Events and Shelf Transport (WEST) project, a 5–year NSF/CoOP-funded study of the role of wind-driven transport in shelf productivity off Bodega Bay (northern California) from $2000 - 2003$. We combine shipboard velocity profiles (ADCP) and water properties from hydrographic surveys during the upwelling season to examine the mean across-shelf structure of the hydrography and velocity fields during three contrasting upwelling seasons, and throughout the upwelling-relaxation cycle. We also present results from two winter seasons which serve as contrast to the upwelling seasons.

During all three upwelling seasons clear spatial structure is evident in velocity and hydrography across the shelf, exemplified by current reversals inshore and the presence of a persistent upwelling jet at the shelf break. This jet feature changes in structure and distance from the coast under different wind forcing regimes. The jet also changes from the north of our region where it is a single narrow jet, adjacent to the coast and to the south of our region where it broadens and at times two jets become evident. We present observations of the California Under Current which was observed at the outer edge of our domain during all three upwelling seasons. The observed across-shelf structure could aid both in the retention of plankton inshore during periods of upwelling followed by relaxation and in the export of plankton offshore in the upwelling jet.

Key words: CoOP WEST, Bodega Bay, Pt Reyes, Relaxation

1 Introduction

In strongly wind forced coastal regions an upwelling paradox exists between the effects of strong wind forcing which can contribute to transport or export out of the shelf region and the presence of high productivity which seemingly results from retention of upwelled material and subsequent algal blooms. In this study we address this paradox by investigating the across-shelf structure in velocity and hydrography in the northern California upwelling region.

The upwelling region off the coast of northern California ($37-40°$N) experiences the strongest summertime wind forcing along the US west coast (*Dorman and Winant*, 1995). This cycle of wind forcing and the upwelling response has been well studied in the past few decades. Large scale studies in the region include the Coastal Ocean Dynamics Experiment (CODE) (*Beardsley and Lentz*, 1987), Northern California Coastal Circulation Study (NCCCS) (*Largier et al.*, 1993), and the Shelf Mixed Layer Experiment (SMILE) (*Dever and Lentz*, 1994; *Dever*, 1997a,b). Hence the dynamics of the region are fairly well described over the course of an upwelling-relaxation cycle (*Hickey*, 1998). *Winant et al.* (1987) identified the persistent upwelling favorable (equatorward) winds during the summer season which are responsible for the onshore transport of cold nutrient rich bottom water and the formation of an 'upwelling center' between Pt Reyes and Pt Arena (*Huyer and Kosro*, 1987; *Lentz and Chapman*, 1989). *Strub et al.* (1987) documented the 'spring transition' at the onset of the upwelling season and *Send et al.* (1987) identified relaxation periods, characterized by poleward flows and surface warming.

* Presently at The University of New South Wales, Sydney NSW, 2052, Australia.
Email address: mroughan@unsw.edu.au (Moninya Roughan).

In this region, (Figure 1) the coastline extends in a relatively straight line southeast from Pt Arena (39°N) to the smaller Bodega headland, (38°20′N D–line) where southward alongshore flows are enhanced during the upwelling season. The flow past Bodega Head drives a re-circulation within Bodega Bay which aids in the retention of crab larvae during periods of upwelling (*Roughan et al.*, 2005). To the south of Bodega Bay the coastline turns sharply to the west to form the large promontory of Pt Reyes (38°N). Pt Reyes is the northern boundary of the Gulf of the Farallones and can act as an 'upwelling shadow' trapping upwelled waters in its lee. The waters that are retained in the lee of the headland are warmed and may return northward towards the region of the 'upwelling center' during relaxation periods when the general alongshore flow reverses (*Send et al.*, 1987; *Wing et al.*, 1995, 1998). The hydrography in the Gulf of the Farallones region to the south of Pt Reyes has been well documented by *Steger et al.* (2000). Offshore and to the northwest of this headland is the submerged Cordell Bank, where the water shallows to a depth of < 90 m. The combination of the submerged bank adjacent to a significant promontory forms an interesting topographic feature which appears to affect the flow field (*Kaplan et al.*, 2005; *Kuebel-Cervantes and Allen*, 2006). This is the focal point for future investigation of the effects of topography on classical upwelling circulation.

Similar upwelling studies have recently been conducted off the Oregon coast (*Barth and Wheeler*, 2005), which contrasts the northern California upwelling region in a number of ways. Most notable is the fact that the upwelling region of northern California is stronger than off the coast of Oregon. Wind forcing is stronger, wind stress curl is greater, and the cycle of upwelling and relaxation is more defined (*Dorman et al.*, 2005). As a result of the stronger forcing, the surface boundary layer is deeper (*Dever et al.*, 2006). As with the case off Oregon we see effects of topography on the upwelling system. The difference however is that

while Heceta Bank (Oregon) is purely a sub-surface feature, in our region, the combination of the prominent Pt Reyes headland and the shoaling Cordell Bank play a dominant role in the circulation in both upwelling (export) and downwelling (retention) conditions.

Previous studies in the northern California upwelling region have focussed on the temporal evolution of alongshore wind forcing and the response of shelf waters (e.g. *Gan and Allen*, 2002a,b; *Dever*, 1997a). Clearly the depth-dependent across-shelf flow is important, particularly where there is velocity shear and counter currents are commonly observed. This study builds on the work of *Huyer and Kosro* (1987) and *Kosro* (1987), conducted during the CODE era. With our data set we are able to extend the observations to the south of the CODE region, to include the waters immediately north of and adjacent to Pt Reyes, as well as to include a multitude of biological observations. Most importantly we are able to examine the effects of the upwelling and relaxation cycle on the biological productivity. This work was undertaken as part of the Wind Events Shelf Transport (WEST) program, which was designed to take an integrated (three dimensional) view of wind forcing and the biological response.

The present study compliments the work of *Dever et al.* (2006) who looked at the surface boundary layer response to wind forcing (from moored observations), and *Kaplan et al.* (2005) who addressed the question of the across-shelf structure of the surface flows (derived from HF radar). In Section 3 we identify the water masses observed in the region and the mean hydrographic conditions across the shelf as measured during both the summer and winter seasons. In Section 4 we identify the pertinent across-shelf features of the depth-dependent flow field in the spring of 2000, 2001 and 2002 (Section 4.1), and also during the winter of 2002 and 2003 (Section 4.2). We focus on shipboard velocity measurements

that were obtained underway during the five WEST cruises and the associated hydrographic structure. With the aid of comprehensive high-resolution Scanfish observations of temperature, salinity and chlorophyll we are able to enhance the three dimensional picture of the across-shelf structure of wind driven upwelling. We use the example of Spring 2001 to investigate the change in across-shore structure along a shore-normal line through the middle of our study site (D–line) throughout the cycle of upwelling and relaxation (Section 4.3). In Section 4.4 we synthesize the results presented and outline the characteristics of the upwelling jet in the WEST region. Our overarching goal is to contribute to the understanding of the paradox of strong wind forcing (transport) and high productivity (retention) across the shelf, hence in Section 5 we discuss the biological implications of the across-shelf structure and relate our findings to other studies in the WEST region.

2 Data Analysis and Methodology

From May 2000 to January 2003 five combined hydrography and biology sampling cruises were conducted from the *R.V. Pt Sur* along the California continental shelf between Point Arena and San Francisco, (Figure 1) as part of the WEST program. There were 3 spring cruises May–June 2000, 2001 and 2002, designed to capture the spring upwelling transition and two contrasting winter cruises; January 2002 and 2003. The spring cruises were one month in duration and consisted of a repeated two week sampling cycle. The sampling cycle consisted of a large-scale survey, a small-scale survey, biological timeseries sampling, underway mapping using a towed profiler (Scanfish) and a second small-scale survey. The goal was to obtain two large-scale surveys and four small-scale surveys during each cruise. The winter cruises were of two weeks duration and were designed to repeat the two-week

sampling cycle conducted during the spring cruises.

The hydrographic sampling was designed along six across-shelf transects with stations located 10 km apart on each line (Figure 1). The array was centered on the D–line, a line running across the shelf, starting at 38°20′ N and 123°4′ W and extending 70 km offshore. The D–line extends shore-normal along a line connecting the primary moored current meter arrays (D040, D090, and D130) and NDBC buoy 46013. Stations started in 15 m water and were spaced 10 km along the line. Stations D 1.5 and 3.5 were added during the first cruise and sampled during each subsequent cruise. The A–line was 40 km to the south and the F–line, situated 40 km north of the D–line, corresponds to the C-line from the CODE experiments of the 1980s. Due to the narrow shelf width, only six stations were occupied on the northern line. The B– and C–lines were 20 and 10 km south of the D–line and the E–line was 10 km to the north. The B–line was seldom sampled and in later cruises was modified to include stations on a diagonal line between Pt. Reyes and Cordell Bank.

The large-scale mapping survey occupied eight A–line, ten D–line and six F–line stations, where the full suite of physical, chemical and biological samples were collected. While the goal was to conduct two full large-scale surveys each cruise, this was often hampered by rough weather conditions. Where possible the Scanfish was deployed and traversed along each of the survey lines.

The shorter small-scale survey, consisting of the inner six stations (10 km apart) on lines (B, C, D and E), were repeated weekly throughout each of the cruises. The ADCP operated continuously during the cruises and the Scanfish deployed whenever there was a reasonably long steam and the weather allowed. Thus the best ADCP lines obtained were measured concurrent with Scanfish lines. During the biology timeseries sampling, Scanfish transects

were run along the D–line, the distance covered dictated by the biology sampling interval. During the winter cruises, the Scanfish operations were curtailed by the large numbers of crab fishing gear deployed on the shelf. The timing of each of the four transects presented here is shown in Table 1.

Five well equipped current and hydrography moorings were deployed, three along the D–line at depths of 40, 90 and 130 m, (D040, D090 and D130 respectively) and two along the 90 m isobath, one north of the D–line (E090) and one south of the D–line (C090) (Figure 1). The data from the moorings are presented in *Dever et al.* (2006) and *Dever and Roughan* (2006), however they are mentioned here for completeness.

2.1 Wind

Wind speed and direction were measured at the NOAA National Data Buoy Center (NDBC) buoy 46013 located at 38.23° N and 123.32° W, in $\sim$ 130 m of water, approximately 25 km from the coast, shore-normal along a line from Bodega Head. Winds were also measured at each of the moorings as described by *Dorman et al.* (2005). Gaps in the NDBC 46013 record were filled through regression with the wind records on the near by WEST moorings. Here we quantify upwelling periods in a classical sense (i.e using wind strength rather than ocean temperature or salinity) and define them as being when the 36 hour, low-pass filtered, equatorward wind strength at NDBC 46013 exceeds 5 ms^{-1}.

Typically winds are strongly upwelling favorable in the summer months, as was observed during May–June 2000 – 2002 (Figure 2). During 2001 wind was strong and upwelling favorable, however was still punctuated by significant periods of relaxation. The mean wind

strength (stress) was ~ 8 ms^{-1} (0.18 Nm^{-2}) southward (*Dorman et al.*, 2005). The summer of 2000 was the weakest of the three upwelling seasons with weaker upwelling favorable velocities and more relaxation periods, where as during 2002 upwelling favorable winds were the strongest and most persistent during the months of May and June. During the winter survey periods winds were weaker and more variable (Figure 3); for example from Jan–April 2002, the mean wind strength (stress) was ~ 1.6 ms^{-1} (~ 0.04 Nm^{-2}) and the standard deviations were large (*Dorman et al.*, 2005). These results are comparable to those found by *Dorman and Winant* (1995) who analyzed 10 years of atmospheric data from NDBC 46013 and found the mean winter strength to be ~ 1.8 ms^{-1} while the summer mean was ~ 6.4 ms^{-1}.

2.2 Shipboard Current Profiles

Underway velocity profiles along the ship track were obtained using a vessel mounted RDI narrowband 150 kHz acoustic Doppler current profiler (ADCP). Measurement ensembles were obtained every 5 min with a vertical bin size of 8 m. The 5 min ensembles were averaged to give 15 min estimates of velocity. Unless otherwise stated velocities are averaged in time rather than space. Bottom tracking was used when the water depth was less than 450 m to estimate relative water velocities, otherwise differential GPS was used. Error estimates in the 5 min velocity ensembles vary from 0.02 ms^{-1} whilst bottom tracking to 0.04 ms^{-1} when using differential GPS for positioning. Unless stated otherwise velocity profiles were decomposed to the alongshore and across-shelf components where the alongshore direction is taken to be 327°, i.e. 33° west of north.

Through analysis of HF radar estimates of surface velocity, *Kaplan et al.* (2005) found that

in the surface waters, fluctuations on a sub-tidal timescale account for $45-75\%$ of the variability, whilst tidal harmonics explained only $4-14\%$ of the total variance in the surface velocity field. *Steger et al.* (1998) found that in the Gulf of the Farallones region individual tidal constituents exhibit considerable spatial variability, i.e. the tides change from mixed to diurnal across the shelf. *Rosenfeld* (1987) investigated the structure of the internal tide in the region and found that it varied in magnitude depending on the phase of the wind cycle (upwelling or relaxation) when stratification was either weaker or stronger. The amplitudes ranged $5-10$ cms^{-1} over the shelf with some surface intensification up to 20cms^{-1} during periods of relaxation. Unpublished data from E. Dever (*pers. comm.*) shows amplitudes on the order of 6 cms^{-1} for both alongshore and across-shelf velocities from timeseries data obtained during the WEST experiments.

Because of the described complexity of the tidal structure, tidal velocities were not removed from the ADCP data. That said, when interpreting the ADCP velocities, one must remember the caveat that tidal forcing will probably have some effect on the instantaneous across-shelf velocities measured with the shipboard ADCP, hence we present averaged velocity sections wherever possible.

2.3 Hydrography

During each cruise hydrographic measurements were made on station with a vertical profiling SeaBird 19 CTD mounted on a General Oceanics 12 bottle rosette sampler as well as underway with another SeaBird 19 integrated into a towed undulating Scanfish. As many as 240 CTD casts were taken on each cruise, primarily at 8 stations on lines A, D and F and 6 stations on lines B, C, and E. CTD data were processed using SeaBird quality control

routines and averaged into 1 m bins. Discrete salinity samples were collected to spot check the CTD data. Only the downcast data are used in this analysis.

The Chelsea Scanfish II is a computer-controlled towed oceanographic instrument designed for underway sampling of the upper 130 m. A SeaBird 19 CTD was integrated into the body, along with a WETStar fluorometer and transmissometer. A Focal Technologies OPC–2T Optical Particle Counter (OPC) was mounted on the center top of the wing. The Scanfish was programmed in an undulating mode allowing underway sampling from the near surface to near bottom across the shelf. The Scanfish was programmed to reverse direction 2 m below the surface and 3 m above the bottom. In deeper water, the maximum obtainable depth was very much sea state dependent. Generally the wing was programmed to reverse vertical direction in the range of $105 - 110$ m. With these settings a complete vertical cycle occurred over an approximate 1.7 km distance. In shallower water the horizontal distance for a complete vertical cycle decreased as water depth decreased. Similar quality control routines were applied and again, data were binned into 1 m intervals for both descending and ascending trajectories. WETStar Fluorometry voltages were converted to $\mu g\, L^{-1}$ based on a regression of the fluorometer incorporated on the rosette mounted CTD and chlorophyll counts from filtered samples collected from the rosette (*Kudela et al.*, 2006).

3 The Distribution of Water Masses over the Shelf

The California coastal region is dominated by two water masses. The cool low salinity Pacific Subarctic Water (PSAW) is transported from the north, by the equatorward California Current (CC). Pacific Equatorial Water (PEW) water is transported to the north by the

poleward California Undercurrent (CUC) (*Steger et al.*, 2000). While the core of the California Current generally lies well offshore of the study region (from the shelf break to 1000 km offshore (*Hickey*, 1998)) portions of the flow can extend into the shelf. Seasonal mean velocities in the CC are about 0.1 ms^{-1} southward (*Hickey*, 1998). Counter to the CC is the California Undercurrent which flows over the over the continental slope along the US west coast. It is strongest at depths of $100-300$ m with peak speeds of up $0.3-0.5$ ms^{-1} (*Hickey*, 1998; *Garfield et al.*, 2001). Although more saline than the CC, the CUC is generally less saline than the inshore waters which are dominated by cold saline upwelled waters during the spring and summer season. Along the coast, river discharge can dilute the salinity of the coastal surface waters. In our region, the Russian River and the San Francisco Bay are the two closest river mouths which could contribute to local salinity modification.

The waters in the study region are a mixture of PSAW and PEW which can be modified by local heating and salinity dilution. Seldom is there a strong front between water masses during the upwelling season and the subtle gradients are best identified using 'spiciness' (*Flament*, 1986), a measure of the distance along an isopycnal between cool fresh water (bland) and warm salty (spicy) waters. In their study of the Gulf of the Farallones, *Steger et al.* (2000) found that the spiciest water was concentrated along the $\sim 26.4\ \mathrm{kg\,m}^{-3}$ density surface within the CUC flowing northward over the slope. This spiciness peak corresponds with the depth of the core of the CUC as measured by Lagrangian Drifters (*Garfield et al.*, 2001). The blandest water further offshore was concentrated around the $25.6-25.8\ \mathrm{kg\,m}^{-3}$ density surfaces. During the spring upwelling surface spiciness was also high due to the warming of upwelled PEW water.

3.1 Seasonal Hydrographic Structure Across the Shelf

Our observations show that the contrast between summer and winter hydrographic conditions is stark, as too is the contrast between shallow waters by the coast, the mid-shelf waters and deep waters over the slope and offshore. Figure 4 shows the mean and standard deviation of temperature, salinity and density from all the spring CTD casts (2000, 2001, 2002) and all the winter CTD casts (2002, 2003). Properties measured from the shore-normal CTD transect along the D–line were averaged into 3 groups across the shelf governed by the proximity to the coast. i.e moving from inshore to offshore the groupings are inner-shelf (D1 -D2), outer-shelf (D3-D4) and slope (D6-D8). The locations of these casts are shown in some of the following figures.

The hydrography of the inner-shelf during spring is clearly different from the conditions observed during winter. During the spring salinity ranges $33.5 - 34$ decreasing with distance offshore and increasing with depth. The most saline waters were found in the upwelled inner-shelf waters, typified by salinity > 33.7. Temperature ranged $8 - 11$ °C in summer, increasing at the outer-shelf, and decreasing with depth. Standard deviation in temperature was up to 2 °C in the surface waters during the spring. This variability in the temperature of the surface waters during the upwelling season is the result of surface heating of the upwelled waters during 2000 (Figure 4) which occurs less in 2001 and 2002. This is evident in the T–S scatter plots for the three spring cruises (Figure 5).

3.2 Inter-Annual Variation in Hydrography Across the Shelf

The T–S scatter plots (Figure 5) show similar hydrographic conditions to those reported by *Steger et al.* (2000), and they also show small differences between each year. Over the shelf and slope the 26.5 $\mathrm{kg\,m^{-3}}$ isopycnal slopes upwards toward the shore, often outcropping. The inner-shelf waters (D1-D2), associated with the upwelled dense water, were the coolest and saltiest and the waters offshore became progressively blander (Figure 5). Surprisingly, during the three summer cruises the inner-shelf waters are comprised of undiluted upwelled PEW water through all stages of the upwelling cycle. It was anticipated that during relaxation events we would see the presence of different water masses, however this was not the case.

In the spring of 2000 we experienced long periods of wind relaxation (Figure 2), during which time surface waters increased in temperature (Figure 5, top row) most likely due to a reduced offshore transport of heat (retention). There was also a lowering of the surface salinity which indicates either the onshore transport of PSAW or the alongshore movement of water diluted by coastal discharge. During 2001 and 2002 we sampled cooler surface waters, with a higher salinity concentration and a narrower range (Figure 5, rows 2 and 3). The minimum surface salinity at the inner-shelf is 33.6, observed during the relaxed period of the 2000 cruise. In 2001 and 2002 the minimum inner-shelf surface salinity was 33.8. This indicates the presence of more upwelled waters and perhaps less retention (i.e. less warming).

The outer-shelf stations (D3–D4) span the transition from the spicy inner-shelf waters to the bland waters at the shelf edge and hence two general surface water types are evident; a denser spicy inshore group and a lower density, blander water further offshore (Figure 5). The highest spiciness inshore was often found at, or south of the D–line, adjacent to the

coast. Maps of surface spiciness show an inshore high, and then a trough of spiciness values trending from nearshore along the F–line to the shelf break on the D–line (Figure 6). Further offshore, the warm surface waters tend to also show elevated spiciness during the spring. The pattern is very similar to the temperature pattern seen in satellite imagery (*Kudela et al.*, 2006).

The lowest density water was found during all three spring cruises at the stations over the slope, but again spring 2000 had the lowest surface densities (< 25 kg m^{-3}) due to lower salinity (< 33.4) and higher temperatures (> 12 °C) (Figure 5).

3.3 Winter Hydrography

During winter the inshore water masses were warmer and significantly fresher than during the spring (Figure 4). There appears to be no PEW up on the shelf, and there is a clear homogeneity across the shelf. The waters of the inner-shelf are nearly identical to the waters found at the outer-shelf and over the slope ($T \sim 12$ °C in waters < 50 m deep). The moored data showed evidence of a wholesale replacement of shelf waters by warmer water (most likely from offshore) during the fall, prior to our winter surveys (E. Dever *pers. comm.*). The biggest contrast during the winter, however, is in surface salinity as there is a significant contribution from terrestrial runoff which acts to lower the surface salinity (Figure 5, rows 4 and 5). This is evidenced by mean surface of $32.5 - 33$ in waters < 50 m deep (in contrast to during the upwelling season, where $S > 33.7$ at the inner-shelf (Figure 4). Surface temperatures offshore were warmer during winter 2003 than in summer 2001 or 2002 (~ 12 °C) and salinities were lower ($32.5 - 33.5$). The T–S diagrams for the two winter cruises (Figure 5, rows 4 and 5) show similar characteristics although there is some variability across the shelf, with 2003

being warmer (by 2 °C) and less saline than 2002, particularly over the slope.

3.4 The Upwelling Front

The surface maps of hydrographic properties (Figure 6) show that there is clear upwelling front (region of low temperature, high salinity) that extends from the north of the region to the south over the inner-shelf. The frontal region appears to widen towards the southern end of the domain. The spatially averaged temperature, and salinity data (Figures 6 and 7) were used to compute geopotential anomaly maps ($m^2\,s^{-2}$) (i.e. the product of the dynamic height (m) and gravity) relative to a depth of 40 m. Traditionally deeper reference levels have been used requiring extrapolation over shallower shelf regions. For this reason reference levels < 100 m have proven useful in shelf regions (e.g. *Barth et al.*, 2000, 2005; *Castelao and Barth*, 2005). While we are able to identify upwelling structures in the shallow shelf waters, absolute estimates of geostrophic velocities are not possible using this technique.

The upwelling front is clearly evident in the surface map of dynamic height (Figure 6), indicated by the region of lower sea surface height adjacent to the coast. What is apparent in the images of temperature, salinity and dynamic height during the upwelling season is a clear delineation between the inner-shelf and the outer-shelf. This gradient extends southwestward (diagonally away from the coast) from north of our study site to south of Pt Reyes. It appears to be co-located with a change in wind stress curl across the shelf as identified by *Kochanski et al.* (2006). This change in surface elevation corresponds with a distinct gradient in salinity at a depth of $10 - 25$ m below the surface as identified in the surface map of salinity (Figure 6), while temperature appears to have a lesser effect on the gradient. During the WEST program, two of the moorings which were deployed were located inshore

of this 'front' (D040 and D090) while the third mooring (D130) appears to have been located at the interface between the two regions. *Dever et al.* (2006) show that surface salinity at the D130 mooring is generally lower than inshore, but the variability is much greater which is in agreement with the idea that as the 'upwelling front' (i.e. the region of lower dynamic height) moves across the shelf during upwelling and relaxation the salinity will change at the stationary mooring. Interestingly the region of highest chlorophyll concentration coincides with the zone of low geopotential anomaly and highest spice. High spiciness indicates that although salinity is high, warming of the upwelled waters has occurred. Hence one could conclude that retention had occurred in this region as the upwelled waters were warmed, and chlorophyll concentrations increased, indicative of a bloom in phytoplankton.

In the winter both the wind stress and the wind stress curl are weaker. High salinity upwelled waters are not present across the inner-shelf and the structure of the temperature, salinity and surface elevation across the shelf is more uniform (Figure 7). Moreover with the decrease in the salinity and increase in temperature, the mean elevation across the shelf is greater in winter than in summer (note the different colorbar scale during winter in Figure 7) and there is no upwelling front, hence no gradient.

4 The Three-dimensional Circulation Patterns over the Shelf and Slope

For wind-driven upwelling systems data have typically been interpreted using a 2–D conceptual model of upwelling. However clear evidence of a more complicated structure is identified by the data obtained during the WEST program. Through temporal averages of HF radar measurements of the surface velocity fields in the WEST region, *Kaplan et al.* (2005) iden-

tified zones in the surface velocity structure across the shelf. Using shipboard ADCP measurements we are able to investigate the across-shelf structure of the depth-dependent flow during wind-driven upwelling and relaxation. We also extend this view beyond the spatial extent of the HF radar domain. While lacking the temporal variability and the statistical confidence of the hourly HF radar time series, using the underway survey velocities and hydrographic characteristics we are able to enhance the radar description by identifying the pertinent features of the depth-dependent flow field and water property distributions.

4.1 The Across-shelf Structure of the Flow Field, Summer 2000-2002

Mean values of selected physical, chemical and biological parameters were calculated for each of 3 lines (F, D and A) for the five cruises; Summer 2000, 2001, 2002 and Winter 2002, 2003. For each parameter the mean values at each location were obtained by simply averaging the individual observations made at the same location during each of the five seasons. We find that the across-shelf structure changes significantly from summer to winter, as expected, and also alongshore from the northern (upstream) end of our region to the southern end of our domain.

4.1.1 F–line

The shore-normal transects of ADCP velocity clearly show a baroclinic pattern across the shelf (Figure 8). During all three upwelling seasons, at the northern end of our domain (F–line) we see strong equatorward flow over the shelf break. During 2001, the core ($v \sim -0.25$ ms^{-1}) was at a distance of $\sim$ 30 km from the coast, with a depth of about 100 m (Figure 8, top row). In 2000 (weaker wind forcing) the core is shallower and weaker ($v \sim$

-0.2 ms^{-1}) than in 2001, and in 2002 (stronger wind forcing) the jet is wider, deeper and stronger ($v \sim -0.3$ ms^{-1}) and further offshore. Inshore of the jet, (< 10 km from the coast) there is evidence of a mean poleward return flow in all three summer seasons with a maximum velocity of $v \sim 0.1$ ms^{-1} in 2002. In 2000 and 2001 poleward flow (the CUC) is evident offshore of the jet (> 40 km from the coast), being stronger and more prevalent in 2000 (weaker wind forcing) and extending inshore under the upwelling jet, as well as to the surface offshore of the jet. The maximum velocity in the core of the CUC (~ 0.25 ms^{-1}) was sub-surface at a depth of ~ 300 m. In 2001, the interface of the jet and the return flow was further offshore (~ 45 km) with a weaker poleward flow maximum ($v \sim 0.15$ ms^{-1}) and a core at a depth of ~ 200 m. In 2002, the poleward flow is seen only at a depth of $300 - 400$ m and > 60km offshore. Across-shore velocities (Figure 8) were weak and directed slightly onshore (positive velocities) in the core of the upwelling jet at the northern end of the domain.

4.1.2 D–line

From north to south the shelf broadens, from a distance of 25 km offshore at the northern F–line to 50 km offshore at the southern A–line, which obviously plays a role in the across-shore location of the upwelling jet. The core of both the jet and the poleward flow are located further offshore in the southern end of our domain, associated with the broadening of the continental shelf. In the middle of the domain we see a similar across-shelf structure to that observed upstream, i.e the presence of an upwelling jet and the CUC offshore. However there are significant differences. At the D-line the upwelling jet may be found offshore or nearshore and it appears that it may be a dual jet structure, with strong velocities appearing offshore and nearshore simultaneously. During the weaker season of 2000, the strongest core is located

50 km offshore, consistent with a pattern in which water is advected south from the upwelling center at Point Arena. During the stronger season of 2002, the maximum alongshore velocities were 25 km from the coast, consistent with a pattern in which the jet was formed locally as a response to local wind forcing. In 2001, the strongest alongshore velocity is again 25 km from the coast, but with a second jet at a distance of 60 km from the coast. This is discussed further in Section 4.3. Along the D–line across-shore velocities are negligible in the jet and inshore, although during 2001, there does appear to be some evidence of onshore flow at the bottom and offshore flow at the surface, reminiscent of a classical upwelling scenario. Offshore, the across-shore velocities are generally negative (away from the shore) and are associated with northward alongshore flow.

4.1.3 A–line

At the southern end of the WEST domain (A–line) we see further evidence of a bifurcation in the upwelling jet, which is most evident in the 2001 transects. The core of the upwelling jet is strongest offshore at a distance of $\sim$ 80 km (2000), and $\sim$ 70 km (2001 and 2002), however we also see evidence of weaker southward flow inshore of this jet during 2000 and 2001, indicating a bifurcation of the upwelling jet. During the strongest upwelling season (2002) the mean northward flow inshore of the upwelling was most pronounced, both in the lee of Point Reyes and also extending offshore beyond the shelf break. Offshore of the shelf the CUC is present, strongest and broadest in 2000, with the only surface expression being in 2001, offshore of the jet. During the stronger season of 2002, the equatorward jet extended down to a depth of more than 300 m.

4.1.4 Hydrography

The across-shore sections of temperature, salinity, density and fluorescence (Figure 9) emphasize the across-shore structure as seen in the velocity sections. Of note is how the depth and the width of the upwelling jet changes, (and hence the changes in the temperature and salinity structure) over the three upwelling seasons. The location of the 8 °C isotherm and the 33.7 isohaline are good indicators of the depth of the upwelled water over the shelf. In each year the F–line has the coldest surface waters. The 8 °C isotherm is at a depth of $50 - 75$ m near the coast along the F–line, but is on average found much deeper ($\sim$ 200m) along the more southerly lines. The coastal waters along the F–line are also more saline over all three years and the 33.7 isohaline marks the off-shore movement of the upwelling front from north to south. The offshore distance of the 33.7 isohaline changes with upwelling intensity, and the strong upwelling season of 2002 exhibits the broadest swath of high-salinity upwelled water. Of note also is the change in fluorescence concentration. The offshore extent of the fluorescence blooms increases from the north to the south end of the domain, with the offshore movement of the upwelling jet. Along the F–line the fluorescence bloom is retained within 40 km of the coast, whereas along the D–line the bloom extends to $\sim$ 60 km offshore. In each of the 3 years we see water property distributions that match the bifurcation of the upwelling jet along the A-line. This is most obvious in the temperature and fluorescence transects of 2000 when there is a coastal bloom in fluorescence as well as a weak bloom $50 - 60$ km from the coast. The most intense blooms that we measured occurred during 2000, the mild upwelling season, and the weakest blooms were during the strongest season (2002), consistent with the idea that periods of relaxation are necessary for blooms to flourish and to be retained. Also evident is the warming inshore along the D–line. It is strongest during 2000 (weak upwelling, more relaxation periods) and absent during 2002 the strongest

upwelling season. The presence of warmer waters inshore indicates retention (and subsequent warming) of high-salinity upwelled waters upstream of Pt Reyes.

4.2 The Across-shelf Structure of the Flow Field, Winter 2002 and 2003

The velocity structures observed during the winter of 2002 and 2003 (Figure 10) differ from those observed during the upwelling seasons. Along the F–line the mean flow over the shelf was poleward during both winter seasons, while the offshore flow was equatorward (in the top 400 m of the water column). In contrast to this, at the D–line the mean flow at the shelf-break was southward and offshore in 2002 and northward and weakly onshore in 2003. In both years there was a weak equatorward flow ($u \sim -0.1$ ms^{-1}) over the inner-shelf and also through the water column at distances over 60 km offshore (veering strongly offshore in 2002). At the southern end of the domain (A–line) the flow was strongly poleward and offshore at a distance of $60-80$ km offshore in 2002. In 2003, however, the poleward flow was weaker and only $40-60$ km offshore, with equatorward flow at depth. The inshore extent of the poleward flow extended further onshore in the winter season (Davidson Current), and the velocity field was weaker ($v \sim 0.1$ ms^{-1} poleward) in the absence of strong equatorward winds.

The winter hydrographic structure (Figure 11) differs greatly from that of summer. The mean depth of the 8 °C isotherm is $250-300$ m along all three lines (A, D and F) during both winters. Mean surface temperatures are warmer than summer (up to 13 °C at the D and A–line in 2003). Surface salinities near the coast are lower in winter than in summer, most likely resulting from freshwater run-off and density is proportionally lower as well (< 25.2kg m^{-3}). The 33.7 isohaline is at a depth of ~ 100 m (versus at the surface during

summer). Isopycnals are generally horizontal across the shelf, with baroclinic forcing found only nearshore associated with land runoff. In contrast to summer, there is an absence of fluorescence in the shelf waters. The zonation across the shelf that was clearly evident during the upwelling season has disappeared and has been replaced by different water masses and different velocity structure.

4.3 Changes in Across-shelf Structure during the Upwelling Cycle, Summer 2001

From our observations, the data obtained during the 2001 upwelling season exhibits the best example of the across-shelf structure through an upwelling-relaxation cycle. It is also the most complete data set that we obtained. Hence we use 2001 as a representative example of the across-shelf structure along the D–line to examine upwelling and relaxation over the shelf and slope and the implications for retention or advection of plankton. We present the alongshore and across-shore velocity structures (Figure 12) and high resolution Scanfish transects (Figure 13) during 3 different phases of the wind cycle as identified in Table 1.

4.3.1 Relaxation: D–line 1

During periods of relaxation (D–line 1, Figure 12) alongshore (across-shelf) velocities were northward (onshore) over the inner-shelf, with a maximum of ~ 0.1 ms^{-1} (~ 0.05 ms^{-1}). This inner-shelf region responded rapidly to reversals in wind forcing. Such flow reversals in this inner-shelf region could aid in the retention of nutrients and plankton while the offshore movement of the upwelling front during periods of strong wind forcing could aid in the export of material from the inner-shelf.

The outer-shelf region ($30-40$ km offshore) was characterized by the presence of a persistent southward upwelling jet through all phases of the wind cycle. During the relaxation period (Figure 12, D–line 1) the jet was narrow and weakly southward ($v < -0.1$ ms^{-1}). The outer-shelf region was flanked by poleward flow over the inner-shelf and offshore, and at the interface, shear zones appear to aid in a deepening of the chlorophyll bloom (Figure 13).

Offshore of the shelf break (more than 45 km from the coast), the persistence of the California Undercurrent (CUC) is evident during both upwelling and relaxation. The CUC is characterized by poleward flow with a subsurface maximum velocity of > 0.3 ms^{-1}. The persistence of the undercurrent is evident, extending to within $50-60$ m of the surface during upwelling. Our observations of the velocity structure show that the upwelling plume weakened and the surface flow over the outer-shelf reversed to a poleward direction. Historically in the literature periods of poleward flow over the slope and outer-shelf have been referred to as a 'surfacing' of the CUC since poleward flow is observed from the surface down into the depths of the consistent CUC flow, with a maximum speed at a depth range of $100-200$ m. However, one needs to be careful when using the term 'CUC surfacing', as typically the CUC consists of PEW, however, during this relaxation period, there was not necessarily an expression of PEW at the surface during offshore poleward flow. Rather it appeared to be a reversal of the flow direction of the surface water.

The position of the zero across-shelf isotach (Figure 12, middle panels) changed with an increase in wind forcing and local topography. During relaxation periods we observed two zero isotachs in the across-shelf velocity. The first at a distance of 30 km offshore at the interface between the inner and the outer-shelf and was identified by a region of zero velocity that extended from the surface (vertically) downward and onshore. The second zero isotach in

the across-shelf velocity, which was less pronounced in the vertical, occurred at the interface between the outer-shelf and the slope region and extended from under the CUC upward to the surface at a distance of $45 - 50$ km offshore.

The Scanfish profiles in Figure 13 show a detailed view of the fine scale structure in the top 120 m. They show the temperature and salinity distribution in the upwelling front and the patchiness in fluorescence across the shelf. Over the inner-shelf region it is evident that stratification in salinity and temperature was weaker during upwelling than relaxation (Figure 13). During relaxation, however, surface warming is observed near the coast (< 8 km offshore), concurrent with a fluorescence bloom. Apart from surface warming, after the onset of upwelling the temperature did not vary greatly in the region close to the coast. *Lentz and Chapman* (1989) found that in this region correlations between wind and surface temperature were lower than correlations between wind and velocity, which indicates that surface heating in the inner-shelf may play a role, however depth averaged heat content and wind forcing were found to be strongly correlated.

4.3.2 New Upwelling: D–line 3

The waters over the mid-shelf transitioned from being barotropic during relaxation to being baroclinic during upwelling. At the onset of upwelling favorable winds (e.g. D–line 3, Figure 12) alongshore and across-shelf velocities over the shelf reversed direction and gradually increased while the upwelling jet over the outer-shelf broadened and strengthened, ultimately merging with the equatorward flow over the inner-shelf (D–line 4).

Through the cycle of relaxation and upwelling the position of the upwelling front (identified in Section 4.1) which forms the boundary of the inner-shelf region, moved offshore as the

upwelling progressed. With this propagation of the upwelling front and the subsequent advection of the upwelling plume are changes in the across-shore structure and in the hydrographic properties as well. The surface became more saline as upwelling progressed (Figure 13) and temperature decreased.

The moored temperature and salinity records (*Dever et al.*, 2006) show that the surface waters at mooring D130 had different hydrographic properties to those at the two inshore moorings. The three moorings along the D–line were located at distances of approximately 1.5, 11 and 28 km offshore, (D040, D090 and D130 respectively), which places D130 at the interface between the inner-shelf and outer-shelf during developed upwelling, or right on the boundary between upwelled water and offshore waters.

One of the noticeable differences during the upwelling cycle was the increase (decrease) in chlorophyll concentration that occurred during upwelling (relaxation) (Figure 13). However, chlorophyll is notoriously 'patchy' during the upwelling cycle and there were large changes in chlorophyll concentration which confound the problem of relating the biological response to wind forcing.

4.3.3 Prolonged Upwelling: D–line 4

At the height of upwelling (e.g. D–line 4, Figure 12) the nearshore flow became baroclinic and offshore flow developed in the surface Ekman layer. The across-shelf flow strengthened ($u > -0.1$ ms^{-1}) and the location of the zero velocity isotach moved offshore (Figure 12, middle panels). The upwelling jet became stronger and broader, but also shallower. The surface waters (< 50 m) across the entire shelf and slope flowed equatorward and offshore over top of the poleward flowing slope waters (at depth). In this upwelling plume (which is

discussed in more detail in Section 4.4), material is advected rapidly southward and retention is less likely.

During upwelling, the extent of the zero across-shelf isotach changed significantly as the upwelling front moved to a distance of $\sim$ 40 km offshore. From our observations it appears that the CUC was subducted underneath the upwelling plume as it grew broader and stronger. At this point the vertical velocity shear increased as the offshore upwelled waters flowed over the top of the poleward flowing CUC.

The shear in vertical velocity was strongest where the equatorward near-surface flow over the outer shelf butts up against the poleward undercurrent over the slope, evident at the offshore extent of our survey line ($>$ 50 km). Following prolonged upwelling winds and the broadening and shoaling of the strong near-surface equatorward flow, this shear zone extends onshore over the shelf to $<$ 30 km. Over the slope, stratification at about 50 m depth appears to be sufficient to withstand this vertical shear (buoyancy frequency, Figure 13), but between 20 and 40 km offshore one can expect active vertical mixing, i.e where the Richardson number ($Ri \sim (N^2/dv/dz)^2$)is less than one. In these locations over the outer shelf, one can also see warm chlorophyll-rich surface waters mixed down $>$ 50 m.

4.4 The Upwelling Jet during WEST

It is now recognized that contrary to the textbook description of upwelling, (where surface flows are offshore during upwelling favourable winds) during wind-driven coastal upwelling an alongshore upwelling jet may form and separation from the coast may occur downstream of the upwelling center (*Barth et al.*, 2000, inter alia). Further, it has been observed that

the California Current may impinge on the shelf through the energetic mesoscale eddy field associated with this current. The eddy energy contribution to the shelf flow from the eddy field can be as large as the energy contribution from local wind forcing (e.g. observations by *Largier et al.* (1993) at the present F–line location). Analysis of satellite data (*Rosenfeld et al.*, 1994) has shown that there are often two paths for upwelled water, one separating offshore and one remaining as an alongshore jet. The dynamics of this separation or bifurcation are not resolved here however, the WEST data builds upon the possibility of two alongshore flow maxima, or 'jets'; one over the inner-shelf which is associated with local wind forcing (weakening or reversing as winds relax), and the other, usually stronger, 'jet' over the shelf break or even further offshore.

This raises the question of whether the offshore jet is a combination of, one, the alongshore upwelling jet streaming down from Pt Arena and two, the interaction with the California Current mesoscale circulation impinging on the shelf and slope. This mesoscale activity may at times move onto the shelf, merging with the waters from the Pt Arena upwelling center and the nearshore coastal jet (e.g. F–line, Figure 8; also *Largier et al.* (1993)) while toward the southern end of our domain the alongshore jet may be well off the shelf, distinct from the nearshore coastal jet (e.g., D–line and A–line, Figures 8 and 12).

The interaction of these dynamical features can result in many flow fields, but off Bodega Bay we see a broadening and shoaling of the two equatorward jets as they strengthen and ultimately merge into a single feature more than 60 km wide (Figure 12, and also D–line in 2002, Figure 8). We present a schematic of these flows in Figure 14, showing the persistent jet found offshore interacting with the poleward undercurrent and the nearshore coastal jet that weakens and reverses during wind relaxations. Inshore of the upwelling plume the SST

schematic shows slightly warmer waters on the northern side of Pt Reyes. In our transects we observed a sporadic northward return flow inshore of the upwelling jet which fascilitates heating and the retention of biological material.

During relaxation it appears that the offshore jet is located over the slope (Figure 12), inshore of a poleward flow that extends to the surface. While elements of this pattern are evident in HF radar data (*Kaplan et al.*, 2005), these data extend less than 45 km offshore. The offshore jet interacts with the undercurrent, with observed strengthening of the undercurrent during years of weak upwelling winds (2000) and weakening or perhaps offshore movement of the undercurrent during strong upwelling years (2002). The interface between shallow equatorward flow and deeper poleward flow is characterized by strong shear and the potential for both diapycnal mixing (when stratification breaks down) and isopycnal mixing along shear surface (when stratification is intact). Along this interface, warm, high-fluorescence water is observed to extend underneath low-fluorescence surface waters to depths greater than 50 m. Downstream at the A–line (Figure 15) this sub-surface chlorophyll maximum feature becomes more apparent. This is consistent with the pattern one would see associated with subduction of high-chlorophyll, aged upwelled waters or with overflow of low-chlorophyll newly upwelled waters at the surface.

The equatorward jets typically transport colder water, more recently upwelled, but with varying levels of chlorophyll fluorescence (e.g. Scanfish data in Figure 13). This surface temperature signal allows the use of satellite imagery in locating the core of the equatorward flows (e.g. Figure 14). Further analysis of composite satellite imagery from our study period is given in *Vanderwoude et al.* (2006) and *Kudela et al.* (2006) and their images exhibit similar characteristics to those identified here. Thus the interaction of the alongshore flow

with the shelf topography and hydrography may lead to the notable thermal signature visible in satellite imagery.

5 The Biological Implications of Variations in Across-Shelf Structure

Upwelling promotes productivity and also enhances export of this production from the shelf. Understanding the relationship between these two effects is a central goal of the WEST program. Here we have shown that the structure of velocity and hydrography varies across the shelf from season to season and with variations in wind forcing. Furthermore, although wind forcing is strong during upwelling conditions, not all the flow is driven by local wind forcing. In addition to affecting hydrographic conditions (and hence nutrient availability) the circulation that develops during upwelling sets the pathways for export. We have shown that export and retention processes during upwelling have complicated three dimensional structures related to the development of an alongshore upwelling front, the local topography, and the presence of distinct offshore and subsurface water masses. We examine export and retention mechanisms in further detail below.

Surface drifters were released during each of the cruises to identify the transport pathways across the shelf. The summer drifter tracks in Figure 16 add to the picture of zonation in circulation patterns across the shelf. In the inner-shelf region there is evidence of retention i.e. a cycle of northward and southward transport during different phases of the wind. At the outer-shelf we see export of the drifters from the region in the upwelling plume, and over the slope region we have both northward transport (in the CUC) and southward transport in the upwelling jet. During relaxation some of the drifters that were released in the lee of

Pt Reyes travelled northward around the headland to land on the rocks on the northern side of the Pt Reyes headland. This northward flow around Pt Reyes has been shown to form a retention area of 'greener', slightly warmer water on the upstream side of Pt Reyes (*Vanderwoude et al.*, 2006).

The structure of the upwelling plume as identified here is consistent with the findings of *Wilkerson et al.* (2006) who measured chlorophyll concentrations and nutrient relationships. Of all the lines surveyed, they found the highest concentrations of phytoplankton along the D–line and suggest that accumulation occurs downstream of the upwelling center. The coldest, saltiest water we observed was along the F–line (upstream), which is consistent with the idea of an upwelling plume which is advected southward away from the coast.

The drifter tracks (Figure 16) and HF radar data (*Kaplan et al.*, 2005) have shown that retention in the inner-shelf region occurs with the changes in wind forcing. This is evident in the ADCP sections that show northward transport in the inner-shelf despite southward flow further offshore. This retention inshore could effectively replenish the inshore environment with nutrients and plankton despite southerly transport further offshore. The retention inshore may lessen the effects of offshore advection during upwelling. While the effects of upwelling and relaxation on nutrient and phytoplankton concentrations in the inner-shelf are relatively straight forward, of particular interest is the associated upwelling plume and the added feature of poleward flowing undercurrent. Depending on the relative depth of the CUC the upwelling plumes may be trapped on the inshore side of the undercurrent or the plume may ride up over the undercurrent (*Garfield et al.*, 2001). In addition, the northward flowing undercurrent exhibits significant shear with the southward shelf circulation and shear instabilities may result in small-scale eddies, observed by *Steger et al.* (2000) over the shelf.

Kudela et al. (2006) investigated the phytoplankton distribution using optical and physical measurements and found that the 200 m isobath served as a clear delineation between coastal and 'oceanic' water masses. While *Lassiter et al.* (2006) found the offshore waters along the D–line to be dominated by nanoflagellates as distinct from the coastal diatom assemblages inshore of 100 m depth. The 100 m isobath defines the location of the upwelling front between the upwelled waters and the offshore waters which are distinguished by oceanic plankton species. The northward flowing CUC may play a role in the retention of plankton on the shelf by reducing further offshore advection of the inshore zooplankton community during upwelling conditions.

The descriptions presented here of velocity and hydrographic structure across the shelf suggest that this structure plays a role in the retention (export) of biological material on (off) the shelf. Further, interactions between shelf circulation and the CUC suggest that the exchange of water both to and from the undercurrent may be a crucial link between circulation and the high productivity over the wind-driven shelf. At the least, large-scale circulation controls on the nature of water entrained in the shelf upwelling circulation will also affect productivity and retention on the shelf.

6 Acknowledgments

We are grateful for the assistance of the captain and crew of the *R.V. Pt Sur*, for their professional execution of all five of our cruises. Many people worked very hard both in the field and in the processing of the data and we are extremely grateful for their dedicated efforts, particularly D. Nelson who operated the Scanfish. We thank C. Collins and T. Chereskin

for their invaluable assistance with the ADCP data. This work was funded by NSF grants 9907884 and 9910896.

References

Barth, J. A., and P. A. Wheeler (2005), Introduction to special section: Coastal Advances in Shelf Transport, *J. Geophys. Res.*, *110*, doi:10.1029/2005JC003124.

Barth, J. A., S. D. Pierce, and R. L. Smith (2000), A separating coastal upwelling jet at Cape Blanco, Oregon and its connection to the Californian Current System, *Deep-Sea Res.*, *47*, 783–810.

Barth, J. A., S. D. Pierce, and R. M. Castelao (2005), Time-dependent, wind-driven flow over a shallow mid-shelf submarine bank, *J. Geophys. Res.*, *110*(C10S05), doi:10.1029/2004JC002761.

Beardsley, R. C., and S. J. Lentz (1987), The coastal ocean dynamics experiment collection: An Introduction, *J. Geophys. Res.*, *92*, 1455–1463.

Castelao, R. M., and J. A. Barth (2005), Coastal ocean response to summer upwelling favorable winds in a region of alongshore bottom topography variations off Oregon, *J. Geophys. Res.*, *110*(C10S04), doi:10.1029/2004JC002409.

Dever, E. P. (1997a), Wind-forced cross-shelf circulation on the northern California shelf, *J. Phys. Oceanogr.*, *27*, 1566–1580.

Dever, E. P. (1997b), Subtidal velocity correlation scales on the northern California shelf, *J. Geophys. Res.*, *102*(C4), 8555–8571.

Dever, E. P., and S. J. Lentz (1994), Heat and salt balances over the northern california shelf in winter and spring, *J. Geophys. Res.*, *99*(C8), 16,001–16,007.

Dever, E. P., and M. Roughan (2006), The depth-averaged momentum balance over the northern california shelf, *J. Phys. Oceanogr.*, *in preparation*.

Dever, E. P., C. E. Dorman, and J. L. Largier (2006), Surface boundary layer variability off northern California, USA during upwelling, *Deep-Sea Res.*, *submitted*.

Dorman, C. E., and C. D. Winant (1995), Buoy observations of the atmosphere along the west coast of the United States 1981 − 1990, *J. Geophys. Res.*, *100*, 16,029–16,044.

Dorman, C. E., E. P. Dever, and J. L. Largier (2005), Buoy measured wind, wind stress and curl of the wind stress over the shelf off Bodega Bay, California, *Deep-Sea Res.*, *in press.*

Flament, P. (1986), Finestructure and subduction associated with upwelling filaments, Ph.D. thesis, University of California, San Diego.

Gan, J., and J. S. Allen (2002a), A modeling study of shelf circulation off northern California in the region of the Coastal Ocean Dynamics Experiment: Response to relaxation of upwelling winds, *J. Geophys. Res.*, *107 (C9)*, 3123, doi: 10.1029/2000JC000768,2002.

Gan, J., and J. S. Allen (2002b), A modeling study of shelf circulation off northern California in the region of the Coastal Ocean Dynamics Experiment 2: Simulations and comparisons with observations, *J. Geophys. Res.*, *107 (C11)*, 3184, doi: 10.1029/2000JC001190,2002.

Garfield, N., M. E. Maltrud, C. A. Collins, T. A. Rago, and R. G. Paquette (2001), Lagrangian flow in the California Undercurrent, an observation and model comparison, *J. Mar. Systems.*, *29*, 201–220.

Hickey, B. M. (1998), Coastal oceanography of Western North America from the tip of Baja California to Vancouver Island, in *The Sea*, vol. 11, edited by A. R. Robinson and K. H. Brink, pp. 345–393, John Wiley & Sons, Inc., New York.

Huyer, A., and P. M. Kosro (1987), Mesoscale surveys over the shelf and slope in the upwelling region near Point Arena, California, *J. Geophys. Res.*, *92*, 1655–1681.

Kaplan, D. M., J. L. Largier, and L. W. Botsford (2005), HF radar observations of surface circulation off Bodega Bay northern California, USA, *J. Geophys. Res.*, *110, C10020.*

Kochanski, A., D. Koracin, and C. E. Dorman (2006), Comparison of wind stress algorithms and their influence on wind stress curl using buoy measurements over the shelf of Bodega

Bay, California, *Deep-Sea Res.*, *in press*.

Kosro, P. M. (1987), Structure of the coastal current field off northern California during the Coastal Ocean Dynamics Experiment, *J. Geophys. Res.*, *92*, 1637–1654.

Kudela, R. M., N. Garfield, and K. W. Bruland (2006), Bio-optical signatures and biogeochemistry from intense upwelling and relaxation in coastal California, *Deep-Sea Res.*, *in press*.

Kuebel-Cervantes, B. T., and J. S. Allen (2006), Numerical model simulations of continental shelf flows off Northern California, *Deep-Sea Res.*, *in press*.

Largier, J. L., B. A. Magnell, and C. D. Winant (1993), Subtidal circulation over the northern Californian shelf, *J. Geophys. Res.*, *98*, 18,147–18,179.

Lassiter, A. M., F. P. Wilkerson, R. C. Dugdale, and V. E. Hogue (2006), Phytoplankton assemblages in the CoOP-WEST coastal upwelling area, *Deep-Sea Res.*, *in press*.

Lentz, S. J., and D. C. Chapman (1989), Seasonal differences in the current and temperature variability over the Northern California Shelf during the Coastal Ocean Dynamics Experiment, *J. Geophys. Res.*, *94*, 12,571–12,592.

Rosenfeld, L. K. (1987), Tidal band current variability over the northern California continental shelf, Ph.D. thesis, Joint Prog. in Oceanogr., Woods Hole Oceanogr. Inst./Mass. Inst. of Technol., Woods Hole, Mass., tech. Rep. WHOI-87-11.

Rosenfeld, L. K., F. B. Schwing, N. Garfield, and D. E. Tracy (1994), Bifurcated flow from an upwelling center: a cold water source for Monterey Bay, *Cont. Shelf Res.*, *14*(9), 931–939.

Roughan, M., A. J. Mace, J. L. Largier, S. G. Morgan, and J. L. Fisher (2005), Sub-surface recirculation and larval retention in the lee of a small headland: A variation on the upwelling shadow theme, *J. Geophys. Res.*, *110*(C10027), doi:10.1029/2005JC002898.

Send, U., R. C. Beardsley, and C. D. Winant (1987), Relaxation from upwelling in the

Coastal Ocean Dynamics Experiment, *J. Geophys. Res.*, *92*(C2), 1683–1698.

Steger, J. M., C. A. Collins, F. B. Schwing, M. Noble, N. Garfield, and M. T. Steiner (1998), An empirical model of the tidal currents in the Gulf of the Farallones, *Deep-Sea Res.*, *45*, 1471–1505.

Steger, J. M., F. B. Schwing, C. A. Collins, L. K. Rosenfeld, N. Garfield, and E. Gezgin (2000), The circulation and water masses in the gulf of the farallones, *Deep-Sea Res.*, *47*, 907–946.

Strub, P. T., J. S. Allen, A. Huyer, R. L. Smith, and R. Beardsely (1987), Seasonal cycles of currents, temperatures, winds and sea level over the northeast Pacific continental shelf: $35° - 48°$N, *J. Geophys. Res.*, *92*, 1507–1526.

Vanderwoude, A. J., J. L. Largier, A. J. Lucas, and R. M. Kudela (2006), Nearshore retention of upwelled waters in northern California embayments - Satellite derived patterns of surface temperature and chlorophyll, *Deep-Sea Res.*, *in press*.

Wilkerson, F. P., A. M. Lassiter, R. C. Dugdale, A. Marchi, and V. E. Hogue (2006), The phytoplankton bloom response to wind events and upwelled nutrients during the CoOP-WEST Study, *Deep-Sea Res.*, *in press*.

Winant, C. D., R. C. Beardsley, and R. W. Davis (1987), Moored wind, temperature and current observations made during Coastal Ocean Dynamics Experiments 1 and 2 over the northern Californian continental shelf and upper slope, *J. Geophys. Res.*, *92 C2*, 1569–1604.

Wing, S. R., L. W. Botsford, J. L. Largier, and L. E. Morgan (1995), Spatial structure of relaxation events and crab settlement in the northern California upwelling system, *Mar. Ecol. Prog. Ser.*, *128*, 199–211.

Wing, S. R., L. W. Botsford, S. V. Ralston, and J. L. Largier (1998), Meroplanktonic dis-

tribution and circulation in a coastal retention zone of the northern California upwelling system, *Limnol. and Oceanog.*, *43*, 1710–1721.

List of Figures

8 Mean alongshore (across-shore) ADCP velocities encompassing all data collected during the Summer of 2000, 2001, and 2002 (L-R) for repeat surveys along the F, D and A–line (top to bottom). The left panels show alongshore velocity (v ms^{-1}) and the right panels show across-shore velocity (u ms^{-1}), where positive velocities are directed poleward (onshore). The locations of the CTD casts along each line are shown by the inverted triangles at the top of each panel, and the D–line moorings are shown by the black triangles in the middle row of panels. 50

9 Mean temperature (°C), salinity (pss) density ($\mathrm{kg\,m}^{-3}$) and fluorescence (volts) encompassing all data collected during the Summer of 2000, 2001, and 2002 (L-R) for repeat surveys along the F, D and A–line (top to bottom). 51

10 Mean alongshore (across-shore) ADCP velocities encompassing all data collected during the Winter of 2002 and 2003 (L-R) for repeat surveys along the F, D and A–line (top to bottom). The panels show alongshore (v ms^{-1}) and across-shore (u ms^{-1}) velocity, where positive velocities are directed poleward (onshore). The locations of the CTD casts along each line are shown by the inverted triangles at the top of each panel, and the D–line moorings are shown by the black triangles in the middle row of panels. 52

11 Mean temperature (°C), salinity (pss) density ($\mathrm{kg\,m}^{-3}$) and fluorescence (volts) encompassing all data collected during the Winter of 2002 and 2003 (L-R) for repeat surveys along the F, D and A–line (top to bottom). 53

Contents

Line	Start Date	Start Time	End Date	End Time	Wind Conditions
A–line 2	22 May 2001	06:16	23 May 2001	11:15	Relaxation
D–line 1	22 May 2001	15:41	22 May 2001	20:17	Relaxation
D–line 3	25 May 2001	23:20	26 May 2001	03:20	New Upwelling
D–line 4	28 May 2001	00:42	28 May 2001	04:36	Developed Upwelling

Table 1
Start and end date and times (UTC) of the concurrent ADCP and Scanfish lines.

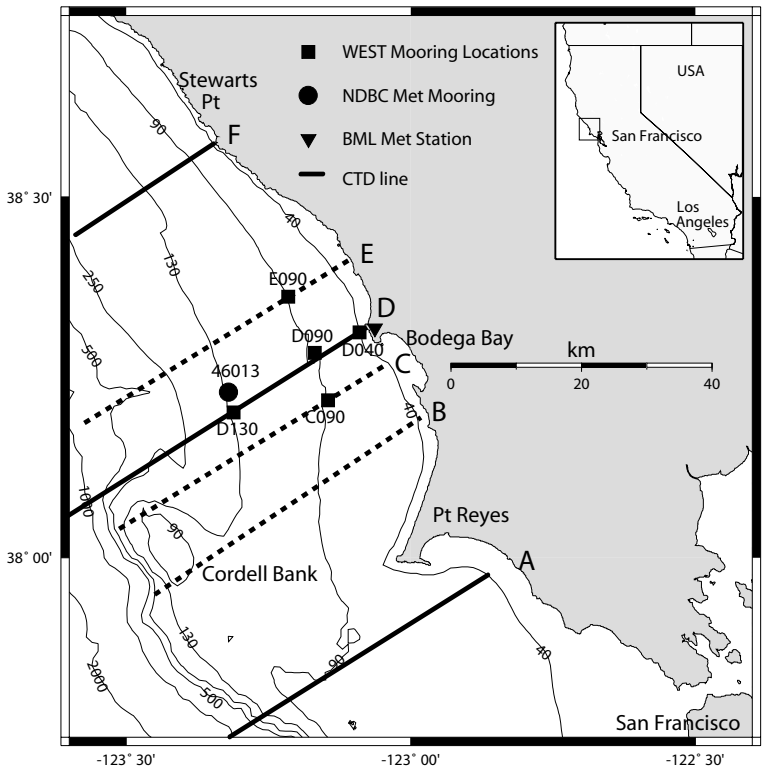

Fig. 1. Map showing the study site; the inset shows the location of the WEST region on the northern Californian coast. The CTD, Scanfish and ADCP transects are indicated by the shore-normal lines, the main lines being A, D, F (solid) and the minor lines B, C, E (dashed). The map is adapted from *Dever et al.* (2006).

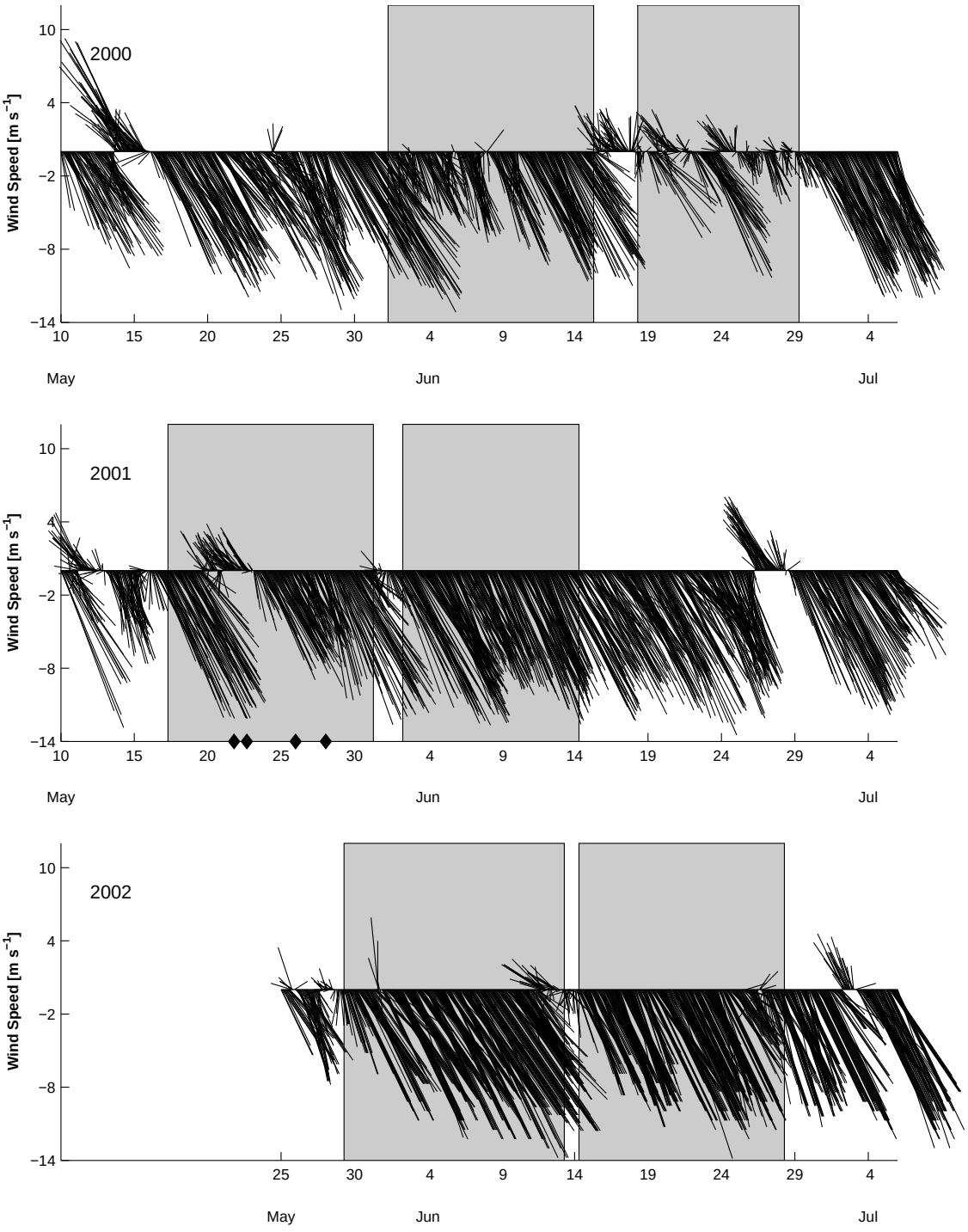

Fig. 2. Wind velocity vectors for spring-summer 2000, 2001, and 2002 (top to bottom). Each of the survey cruises are indicated by the shaded regions. The timing of survey lines during 2001 are identified by the diamonds, from L-R A–line 1, D–line 1, D–line 3, D–line 4.

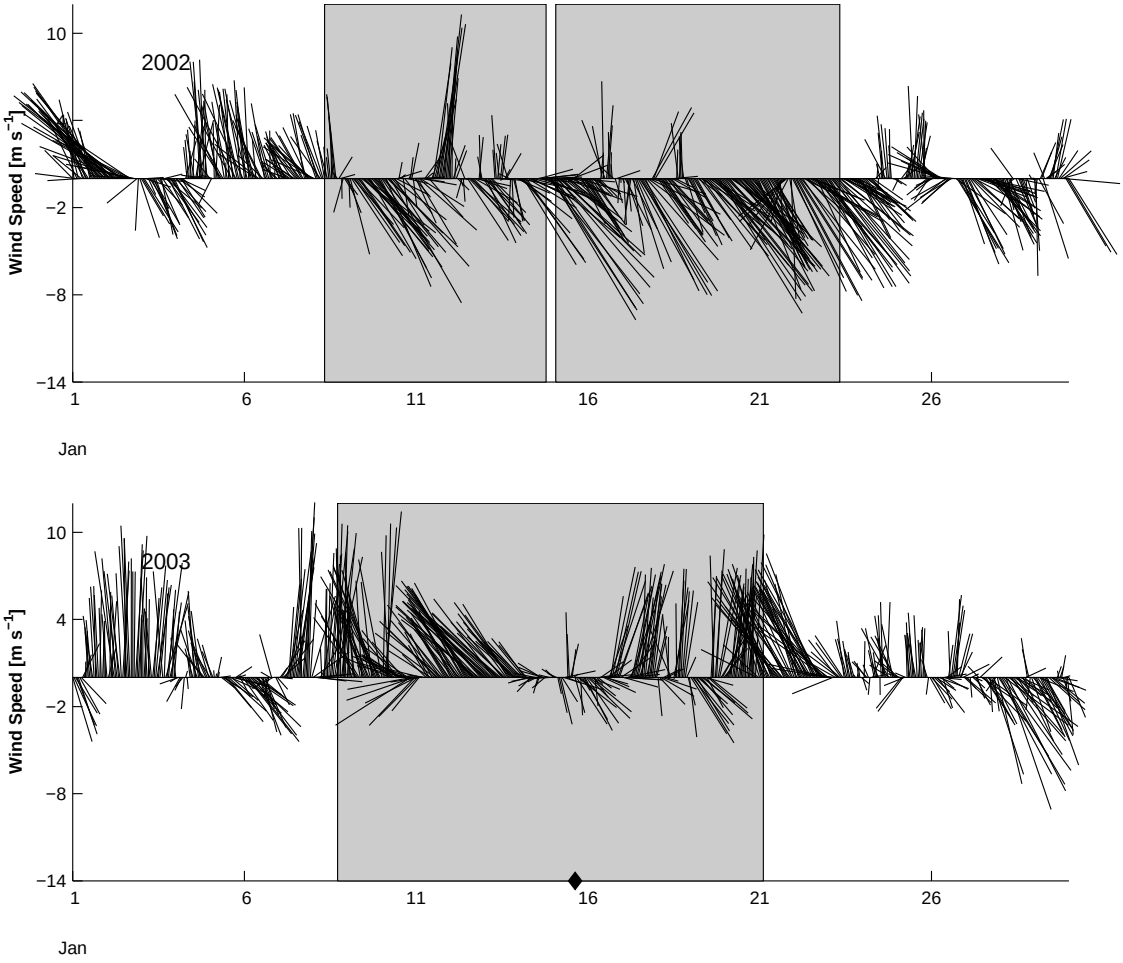

Fig. 3. Wind velocity vectors for Winter 2002 and 2003 (top to bottom). Each of the survey cruises are indicated by the shaded regions. The timing of the survey line at D–line 2 (winter) is indicated by the diamond in 2003.

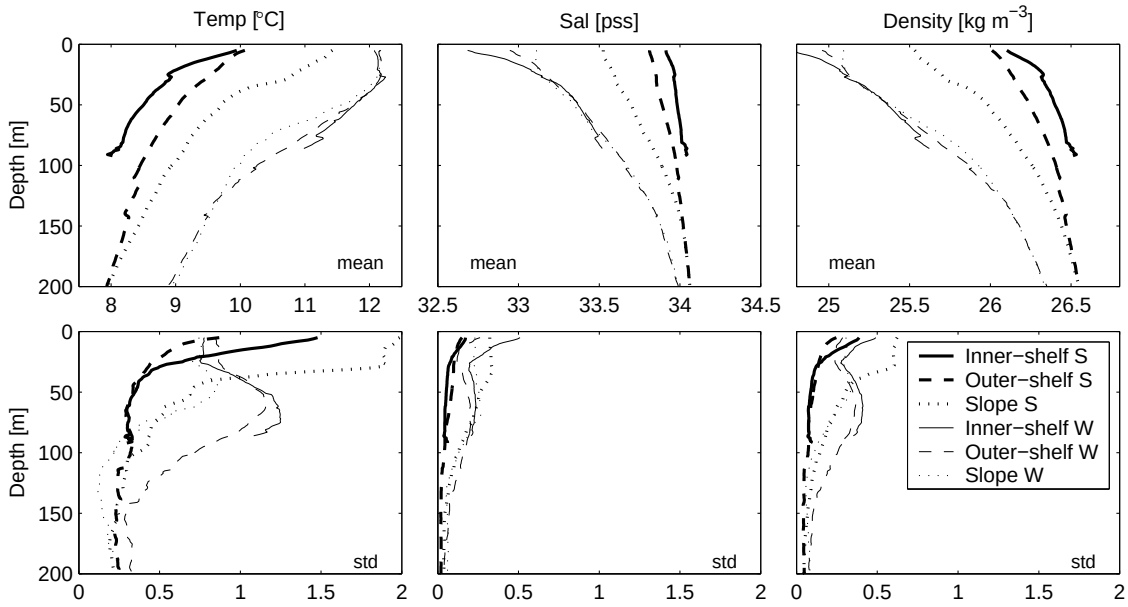

Fig. 4. Mean (top row) and standard deviation (bottom row) of temperature, salinity and density (left to right) in the 3 regions across the shelf: slope (dotted), outer-shelf (dashed), and inner-shelf (solid), using all data from all years, during spring-summer (S - thick lines) and winter (W - thin lines).

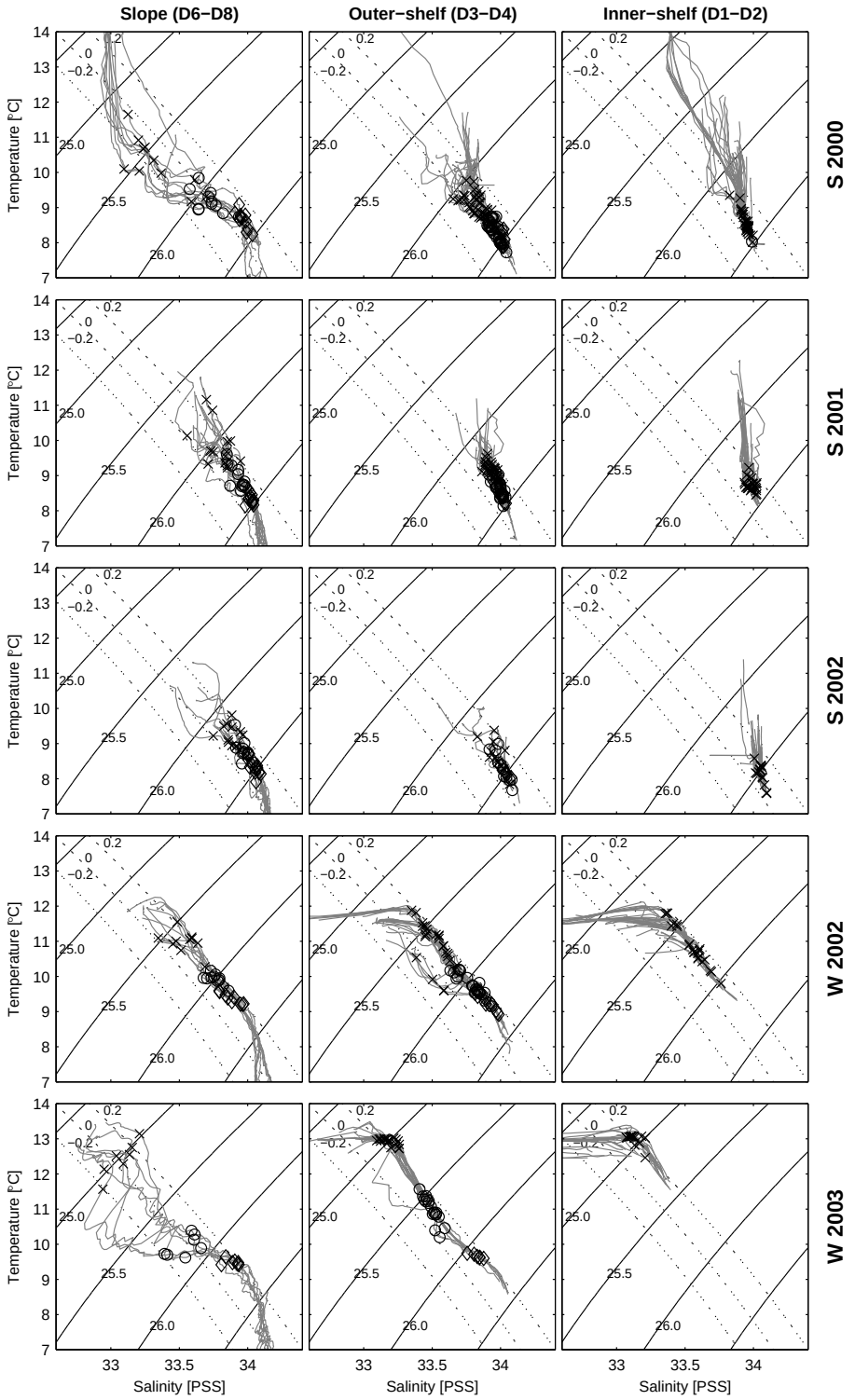

Fig. 5. T–S diagrams for all data acquired during the spring of 2000, 2001, 2002 and from winter 2002, and 2003 (from top to bottom) over the slope D6–D8 (left) at the outer-shelf, D3–D4 (middle) and at the inner-shelf, D1–D2 (right). Each panel shows the temperature – salinity relationship as well as density (solid lines, lower left to upper right) and spiciness (dotted lines, lower right to upper left). The depths of the T–S properties are marked at depths of 50 (cross), 100 (circle) and 150 m (diamond).

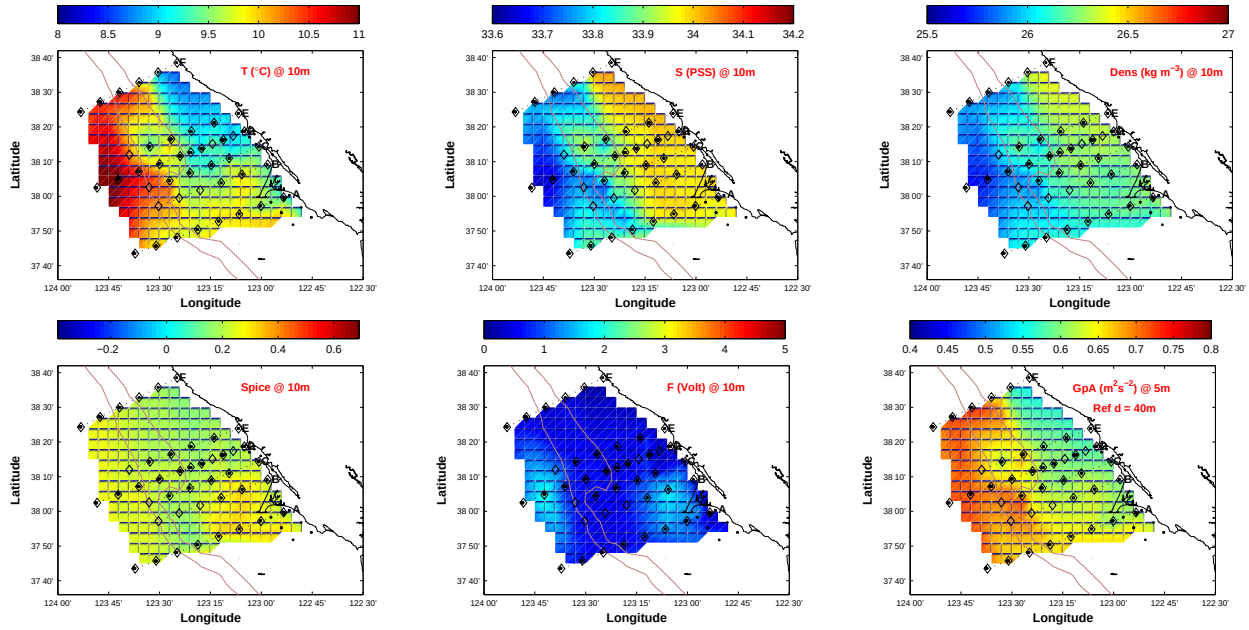

Fig. 6. Surface maps (at a depth of 10 m) of Temperature (°C), Salinity, Density (kg m^{-3}), Spice, Fluorescence (Volts) and Dynamic height at 5 m (relative to a level of no motion of 40 m) from CTD casts during summer 2001. The diamonds show the location of the CTD casts and the black dots indicate that data was used to calculate the dynamic height.

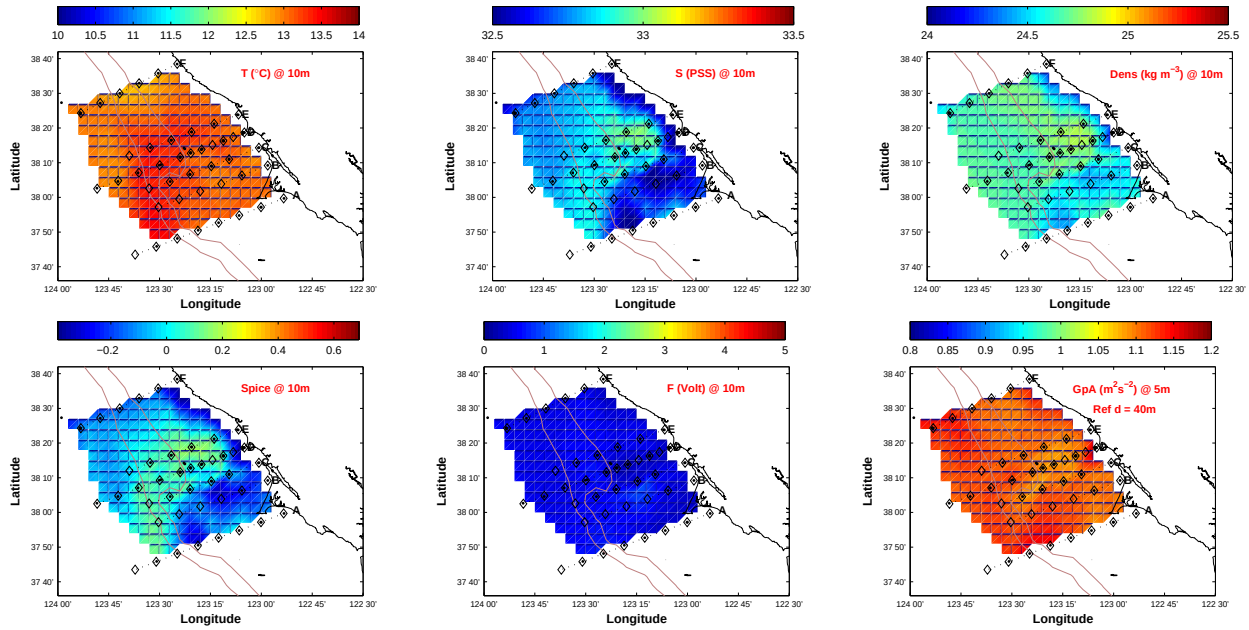

Fig. 7. Surface maps (at a depth of 10 m) of Temperature (°C), Salinity, Density (kg m^{-3}), Spice, Fluorescence (Volts) and Dynamic height at 5 m (relative to a level of no motion of 40 m) from CTD casts during winter 2003. The diamonds show the location of the CTD casts and the black dots indicate that data was used to calculate the dynamic height. Note the colorbar scales differ from those used for the summer surveys.

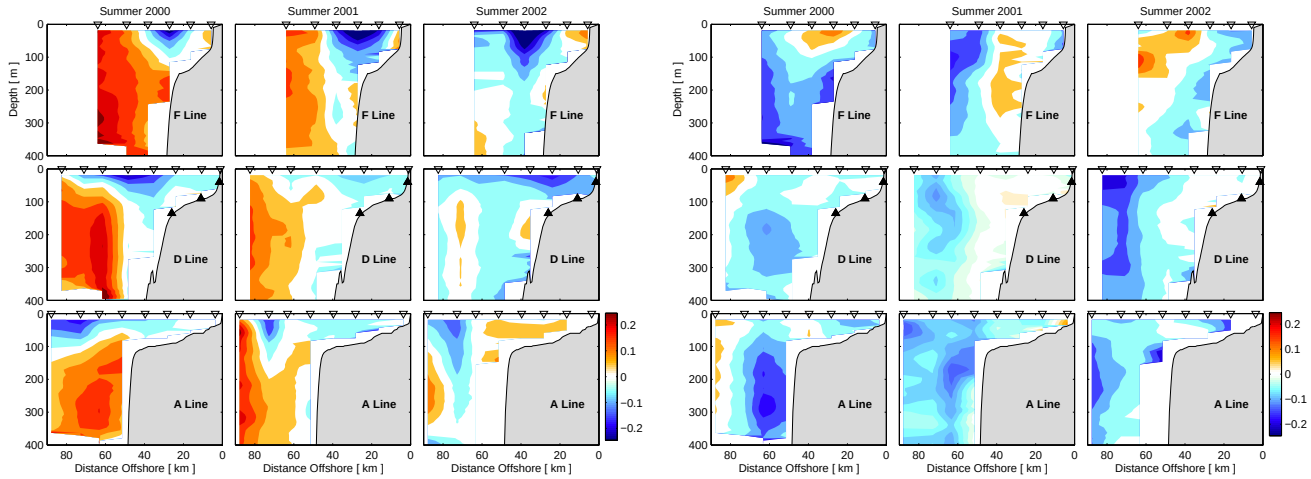

Fig. 8. Mean alongshore (across-shore) ADCP velocities encompassing all data collected during the Summer of 2000, 2001, and 2002 (L-R) for repeat surveys along the F, D and A–line (top to bottom). The left panels show alongshore velocity (v ms^{-1}) and the right panels show across-shore velocity (u ms^{-1}), where positive velocities are directed poleward (onshore). The locations of the CTD casts along each line are shown by the inverted triangles at the top of each panel, and the D–line moorings are shown by the black triangles in the middle row of panels.

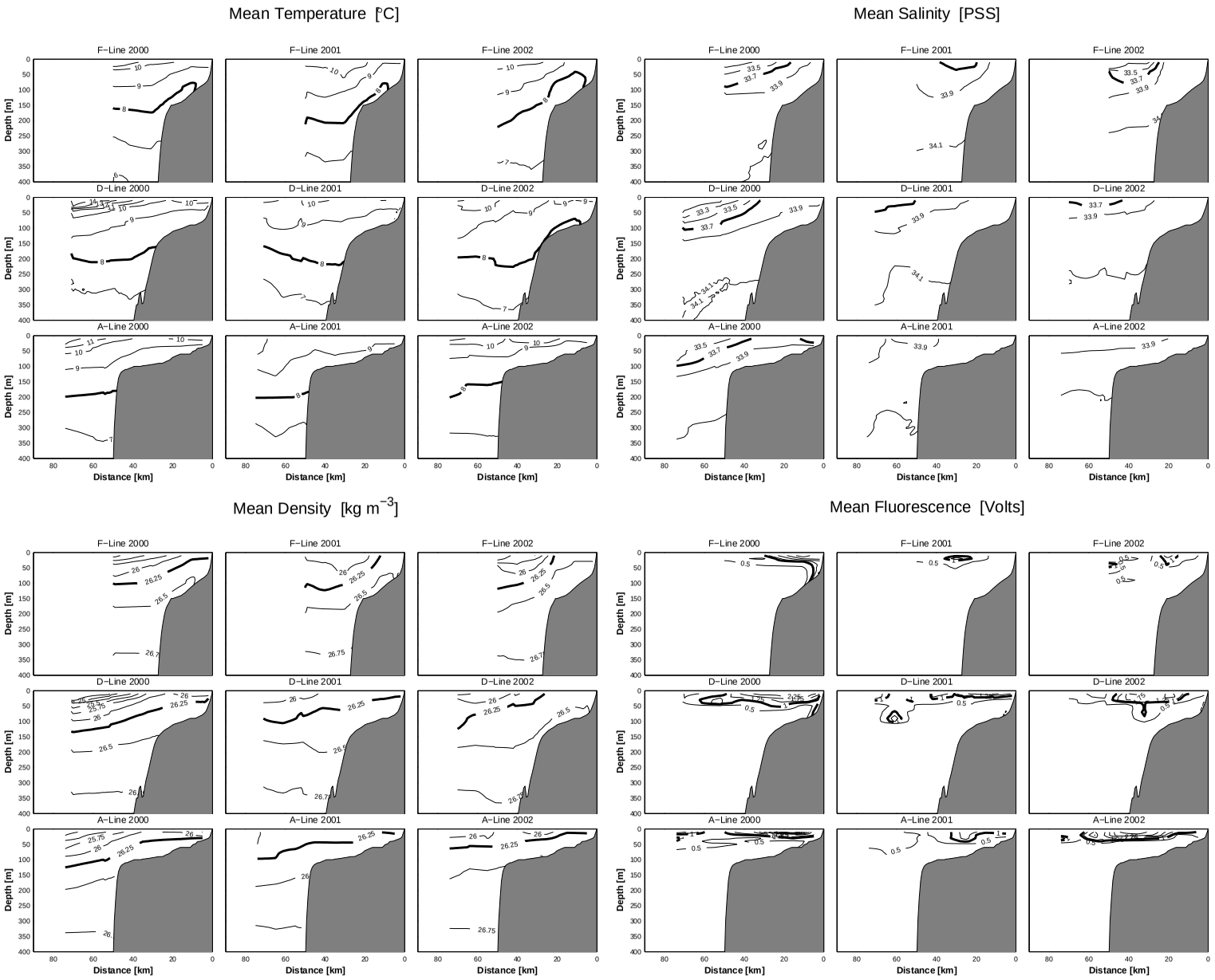

Fig. 9. Mean temperature (°C), salinity (pss) density (kg m^{-3}) and fluorescence (volts) encompassing all data collected during the Summer of 2000, 2001, and 2002 (L-R) for repeat surveys along the F, D and A–line (top to bottom).

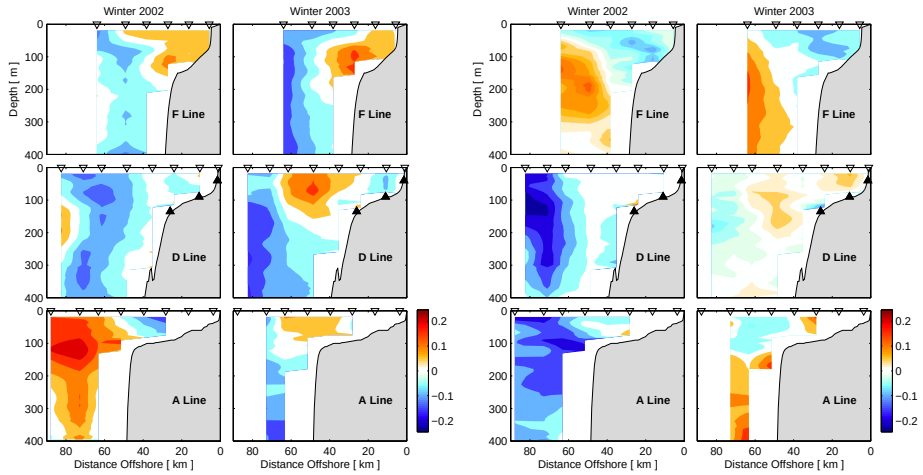

Fig. 10. Mean alongshore (across-shore) ADCP velocities encompassing all data collected during the Winter of 2002 and 2003 (L-R) for repeat surveys along the F, D and A–line (top to bottom). The panels show alongshore (v ms^{-1}) and across-shore (u ms^{-1}) velocity, where positive velocities are directed poleward (onshore). The locations of the CTD casts along each line are shown by the inverted triangles at the top of each panel, and the D–line moorings are shown by the black triangles in the middle row of panels.

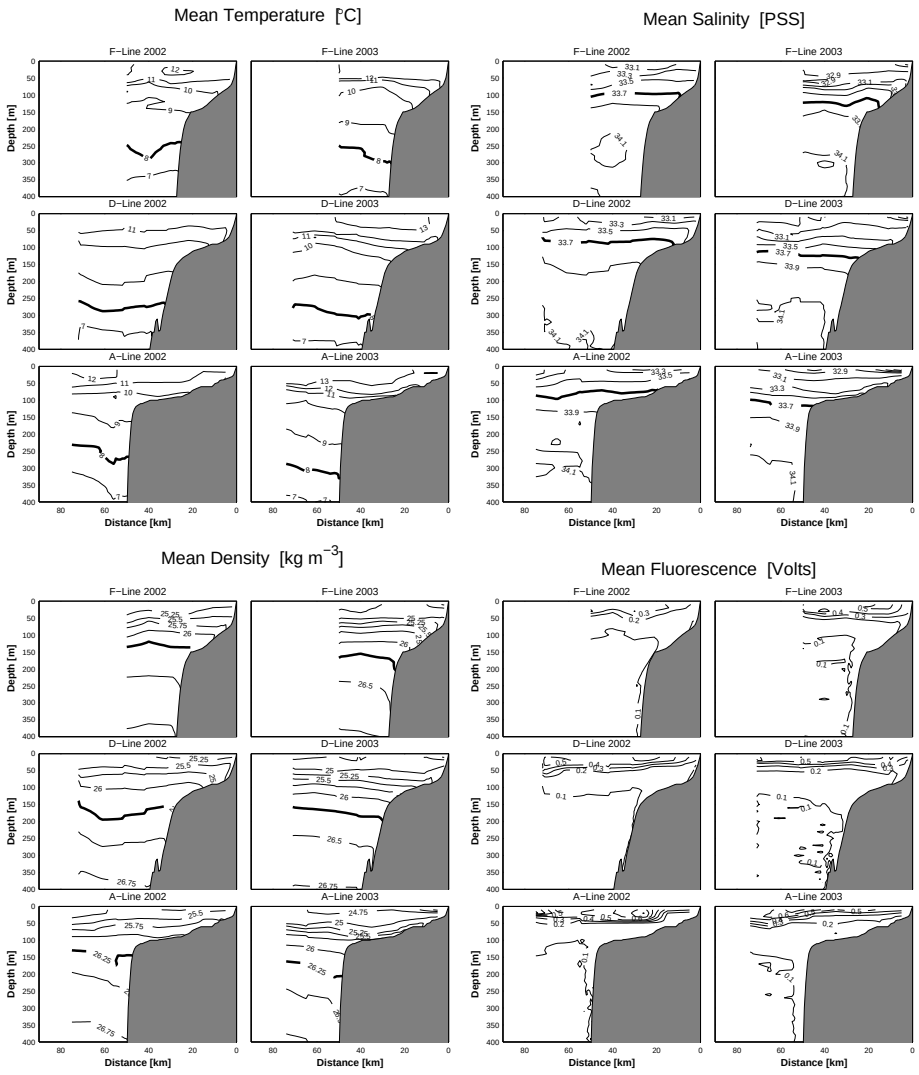

Fig. 11. Mean temperature (°C), salinity (pss) density (kg m^{-3}) and fluorescence (volts) encompassing all data collected during the Winter of 2002 and 2003 (L-R) for repeat surveys along the F, D and A–line (top to bottom).

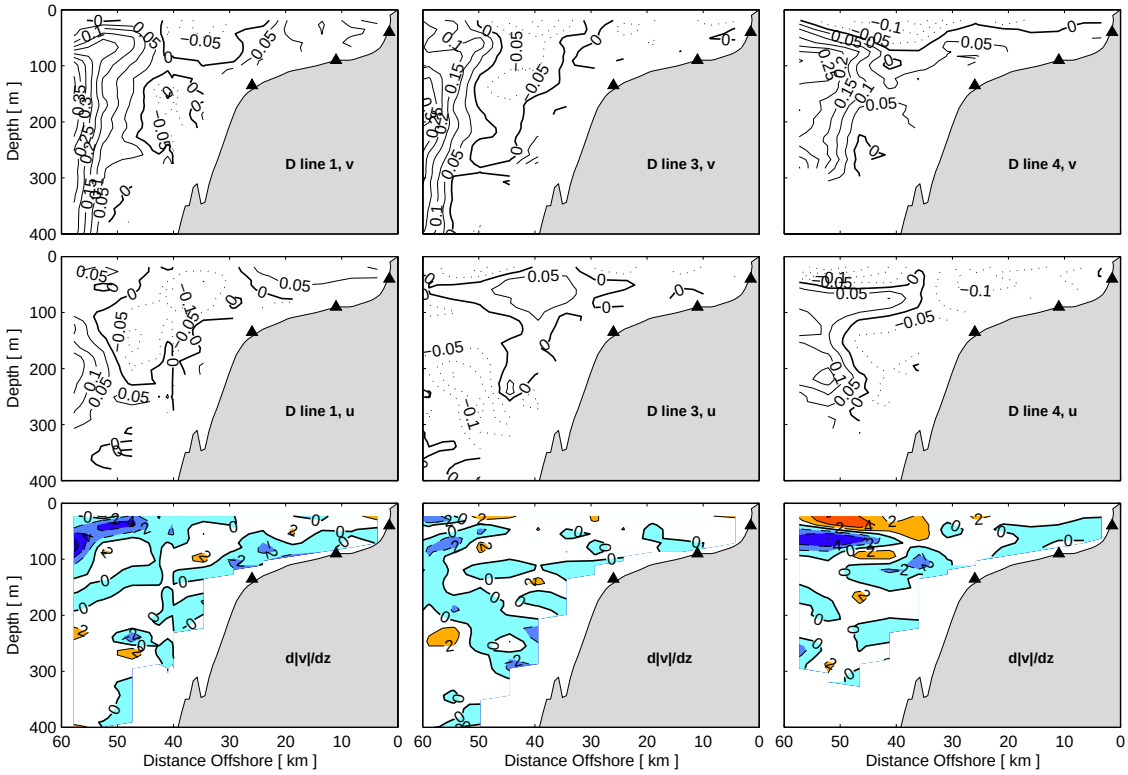

Fig. 12. ADCP velocities for repeat surveys along the D line during relaxation (D–line 1), new upwelling (D–line 3) and developed upwelling (D–line4). The dates and times of each line are given in Table 1. From top to bottom the panels show alongshore velocity (v ms^{-1}), across-shelf velocity (u ms^{-1}) and vertical velocity shear $d|v|/dz$ in units of 10^{-3}s^{-1}. Note that positive alongshore (across-shelf) velocities are directed poleward (onshore). The locations of the D–line moorings are shown by the black triangles.

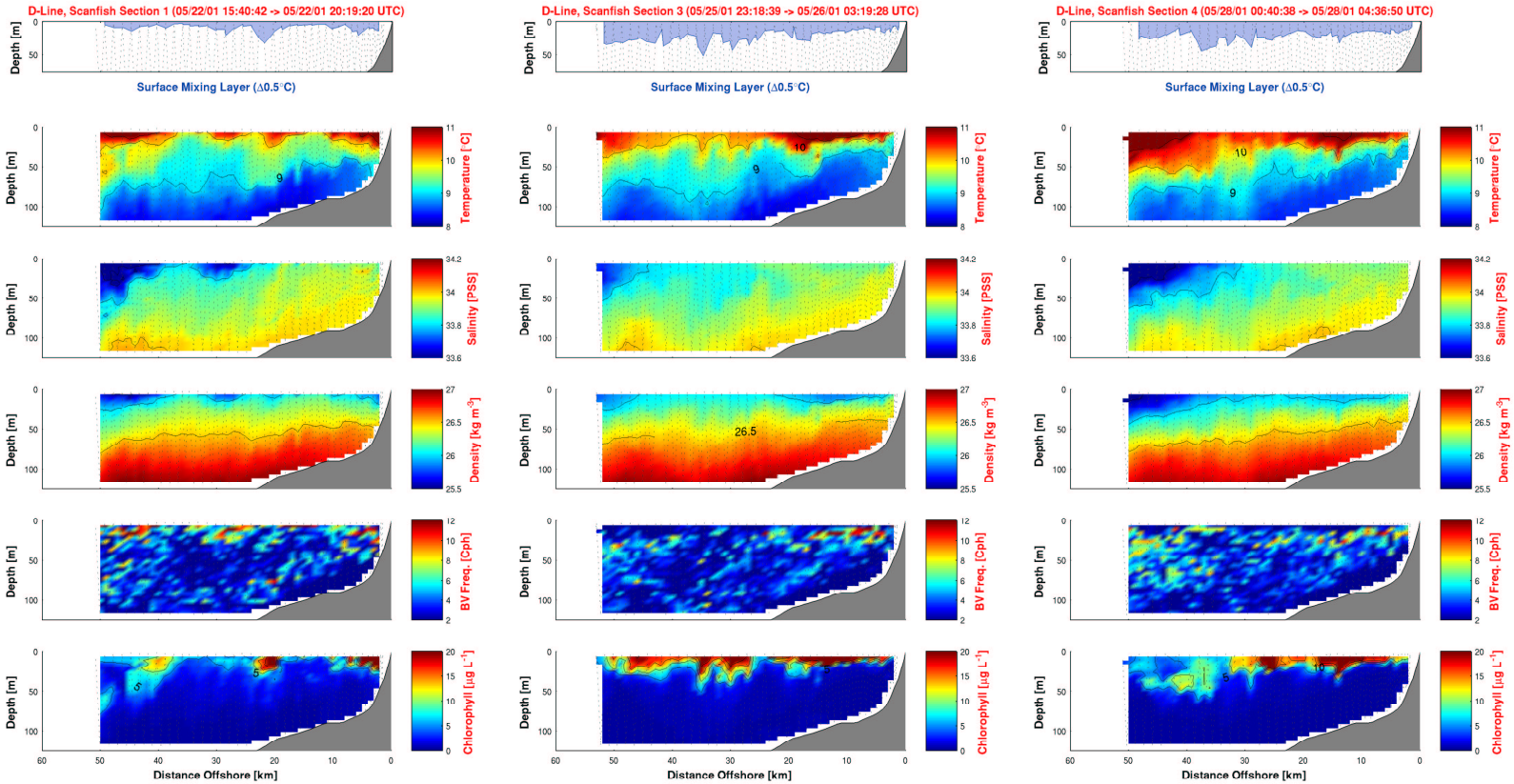

Fig. 13. Scanfish transects: D–line 1 on 22 May 2001 after a period of relaxation, D–line 3 on 26 May after the onset of upwelling favourable winds, D–line 4 28 May during a period of prolonged upwelling favourable winds. From top to bottom, the panels show; Surface Mixed Layer, Temperature (°C), Salinity (pss), Density ($\mathrm{kg\,m^{-3}}$) BV Frequency (cph) and Chlorophyll ($\mu\mathrm{g\,L^{-1}}$).

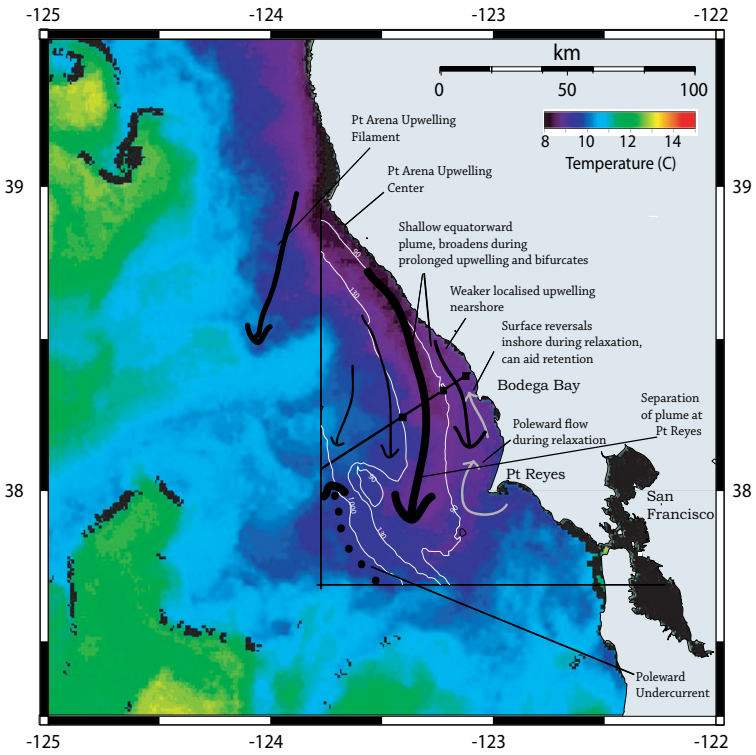

Fig. 14. Schematic diagram of the velocity field during the upwelling season overlaid on a satellite image of sea surface temperature from June 8 2002 03:07 GMT from the NOAA-15 AVHRR sensor, processed using the CoastWatch MCSST algorithm. The arrows show the zonation across the shelf, the alongshore advection of the plume and the retention over the inner-shelf (during relaxation). The thin white lines show the bathymetry within the study site.

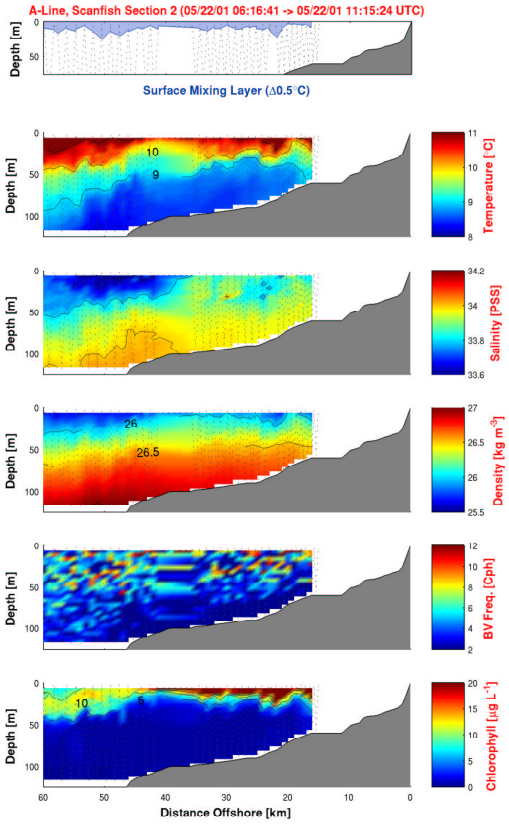

Fig. 15. Scanfish transect along the A–line on 22 May 2001. The panels show the same properties as those in Figure 13.

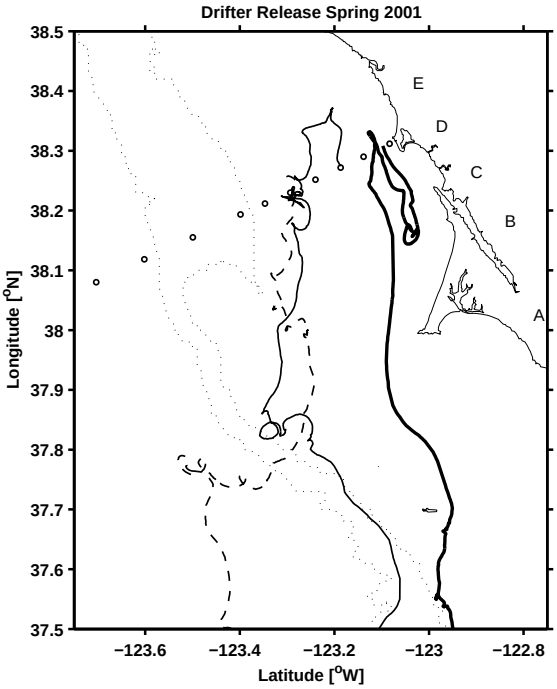

Fig. 16. Drifter trajectories from 3 deployments around 22 May 2001. The solid lines represent deployments over the inner-shelf and the dashed line represents a deployment over the outer-shelf. Note the reversal in direction (and retention) in the inner-shelf and the eventual offshore (southward) transport in the upwelling plume. The 200 and 1000 m isobaths are indicated by the dotted lines and the small circles represent the location of the CTD casts along the D–line.